TITLE: Cine balanced fast field echo magnetic resonance imaging of canine spinal arachnoid diverticulae pulsation

AUTHORS: S.K. Shivapour, H.A. Volk, V. Watts, S. De Decker

JOURNAL: Veterinary Journal

PUBLISHER: Elsevier

PUBLICATION DATE: 29 April 2019 (online)

DOI: https://doi.org/10.1016/j.tvjl.2019.04.014

Original Article

Cine balanced fast field echo magnetic resonance imaging of canine spinal arachnoid diverticulae pulsation

S.K. Shivapour, H.A. Volk, V. Watts, S. De Decker*

Department of Veterinary Clinical Science and Services, Royal Veterinary College, University of London, Hawkshead Lane, North Mymms, Hertfordshire AL97TA UK

* Corresponding author: Tel.: +44 (0)1707 666365
E-mail address: sdedecker@rvc.ac.uk (S.De Decker).

Highlights

- Cine balanced fast field echo MRI sequences identified spinal arachnoid diverticula (SAD) pulsation in dogs
- Significant differences were demonstrated between minimum and maximum SAD dimensions on sagittal and transverse sequences
- Syringomyelia in association with a SAD was observed in 6/12 cases
- No significant association was identified between SAD pulsation on cine balanced fast field echo MRI and extent of syringes

Abstract

Canine spinal arachnoid diverticulae (SAD) are characterised by focal cerebrospinal fluid dilatations within the subarachnoid space, most commonly associated with nonpainful paresis and ataxia secondary to chronic compressive myelopathy. Numerous imaging techniques have been described for diagnosis of this condition, including myelography, computed tomography myelography, and magnetic resonance imaging (MRI). The present retrospective study investigated the utility of cine balanced fast field echo (cine bFFE) MRI sequences in measuring pulsatile flow in 12 dogs with SAD. The secondary aim was to determine the prevalence and location of syringes in relation to SAD, as the co-occurrence of these conditions has not been previously reported.

The degree of SAD pulsation was calculated as the change in area per cardiac cycle on sagittal (*n*=12/12) and transverse (*n*=7/12) cardiac-gated cine bFFE MRI sequences. Pulsation was identified on all sequences, with a median ratio of change in SAD area of 0.14 (range, 0.10 – 0.27; *n*=12) on sagittal cine bFFE and 0.23 (range, 0.05 – 0.53; *n*=7) on transverse cine bFFE sequences. Significant differences between minimum and maximum SAD dimensions were identified on sagittal (*P*=0.002) and transverse measurements (*P*=0.018). A moderate prevalence of syringomyelia was identified (*n*=6/12; 50%) on T2W sequences, occurring both cranial (*n*=4/12; 33%) and caudal (*n*=2/12; 17%) to the SAD. These results support the ability of cine bFFE sequences to identify dynamic pulsation of canine SAD. This technique is currently limited by banding artifacts and its inability to quantify flow velocity and abnormal flow jets.

Keywords: Neuroradiology, cine MRI, syringomyelia, cerebrospinal fluid hydrodynamic

Introduction

Canine spinal arachnoid diverticulae (SAD) are focal dilatations of the subarachnoid space with cerebrospinal fluid (CSF), which may be primary or secondary in origin (Rylander et al., 2002; Lowrie et al., 2014; Mauler et al, 2014). The pathophysiology of SAD is uncertain, although primary or congenital lesions are believed to occur subsequent to splitting of the arachnoid membrane in embryonic development, thereby allowing for progressive expansion of the defect and chronic compression of the underlying spinal cord (Gnirs et al 2003; Lowrie et al., 2014). In acquired cases, canine SAD have been linked to other myelopathies, including intervertebral disc extrusion, vertebral malformation, spinal cord trauma, prior spinal surgery, or inflammatory myelopathies (Galloway et al., 1999; Mauler et al., 2014; Rylander et al., 2002; Skeen et al., 2003).

Multiple techniques have been described in the veterinary literature for the diagnosis of SAD, including myelography, computed tomography (CT) myelography, and magnetic resonance imaging (MRI) (Galloway et al., 1999; Mauler et al., 2014; Skeen et al., 2003). These modalities have led to the characterisation of SAD as having a classic 'tear-dropped' shape on myelography, CT myelography and MRI (Gnirs et al, 2003; Mauler et al., 2014), and resulted in the hypothesis that the anomalous accumulation of CSF may result from a flow disturbance due to a one-way valve located within the diverticulum (Bentley et al., 1991; Dyce et al., 1991; Gage et al., 1968; Parker et al., 1983).

In the fields of human neurosurgery and neuroradiology, attempts have been made to better characterise the CSF hydrodynamics within SAD. Given that conventional MRI sequences do not allow for evaluation of pulsatile movement of the neural architecture within the subarachnoid space (SAS), cine balanced steady state free precession MRI has been utilised

to evaluate cases of idiopathic syringomyelia (SM), allowing for the identification and successful treatment of underlying causes, including arachnoid bands, which are otherwise unidentifiable on conventional MRI subsequent to motion artifact (Gottschalk et al., 2010; Li et al., 2015). Proposed clinical applications of this technique include diagnosis of SAD, idiopathic SM, and pre- and post-operative evaluation of Chiari Type I malformation (Gottschalk et al., 2010; Li et al., 2015).

Currently, the only study in the veterinary literature to evaluate pulsatile flow using cine balanced fast field echo (bFFE) MRI was performed to examine pulsation of the cerebellum in Cavalier King Charles Spaniels with and without SM compared to controls (Driver et al., 2013). No prior reports exist whereby the pulsatile flow within a SAD have been established, nor the degree of pulsation quantitatively measured.

Furthermore, although there are several reports of concurrent SM and SAD in both the veterinary and human literature (Kim et al., 2009; Holly et al., 2006; Mauler et al., 2014; Skeen at al., 2003), the prevalence of syringes secondary to SAD remains unknown. In human medicine, the incidence of SM in patients with SAD is similarly undefined, although is believed to be rare (Kim et al., 2009; Takeuchi et al., 2003). It has been proposed that altered CSF flow within the diverticulae results in the formation of syringes (Kim et al., 2009; Holly et al., 2006), although this hypothesis has not been further investigated.

The primary aim of the present study was to evaluate the utility of cine balanced fast field echo (bFFE) MRI in measuring the dynamic component of canine SAD pulsation. The secondary aim was to assess the prevalence and location of SM in the population under study,

and to examine the relationship between the degree of pulsatile flow identified on cinematic MRI and the extent of SM observed on conventional T2W MRI.

Materials and methods

This study was approved by the Royal Veterinary College ethical and welfare committee (SR2018-1612).

Animals

Dogs were identified for inclusion via search of the Royal Veterinary College (RVC) VetCompass electronic veterinary patient database. Search terms included 'spinal arachnoid diverticula' and 'subarachnoid diverticula.' A total of 29 client-owned dogs with a diagnosis of SAD based upon conventional MRI were identified. Criteria for inclusion in the study were the diagnosis of spinal arachnoid diverticula by a board-certified neurologist based upon clinical presentation and advanced imaging, including conventional MRI sequences and cine balanced fast field echo (bFFE) MRI in at least one plane.

Of the 29 dogs diagnosed with SAD, 12 client-owned dogs were identified which satisfied the criteria for inclusion between May 2009 and June 2018. Descriptive data for all canine patients was recorded, including age, breed, sex, presenting complaint, neuroanatomic localisation, and imaging diagnosis.

Imaging technique

A 1.5 Tesla MRI unit (Phillips Intera) with a 5-element phased-array spinal coil was utilised to acquire all images. All imaging was performed under general anaesthesia using a standard protocol. All dogs were positioned in dorsal recumbency with the head and neck in neutral position and the vertebral column aligned as straight as possible. To facilitate

retrospective cardiac gating and minimise susceptibility artefact, vector electrocardiography was utilised throughout collection of all cine bFFE MR images.

All dogs initially underwent a conventional MRI protocol requisite to obtain a clinical diagnosis of SAD. Identification of concurrent myelopathies (e.g. intervertebral disc extrusion/protrusion, vertebral malformation) were not considered reason for exclusion in the present study, given that the co-existence of these conditions in close proximity has been previously well-documented, particularly in the Pug and French Bulldog (Mauler et al., 2014). The protocol included sagittal and transverse T1 and T2-weighted turbo spin echo (TSE) sequences of the cervical and/or thoracic spinal cord segments, depending on the region affected.

Following diagnosis of SAD, a sagittal bFFE sequence was performed over 20 heart phases with a time to repeat (TR) of 12 ms, a time to echo (TE) of 6.0 ms, 2 mm slice thickness, 50-degree flip angle, pixel size of 0.7 mm x 0.7 mm, 220 mm x 126 mm field of view, and 316 x 180 acquisition matrix. In seven of twelve cases, a second bFFE sequence was performed in the transverse plane over the region of maximal SAD dilatation. The acquisition time per bFFE scan was approximately 3 min, although some scans required several attempts to minimise repetition, banding, and ghosting artifacts. In those cases where multiple scans were obtained, the scan with the fewest artifacts in the region of interest was selected for analysis. See the supplementary videos for examples.

Imaging analysis

Conventional T2W and cine bFFE image sequences for each dog were loaded into open source DICOM viewing software[1] for analysis. Diagnosis of a subarachnoid diverticulum was confirmed by a board-certified neurologist (SDD), and was defined as a focal dilatation of the subarachnoid space with cerebrospinal fluid (Mauler et al., 2014). Syringomyelia (SM) was identified as a fluid-filled cavitation within the spinal cord parenchyma with an internal diameter of >2 mm or greater (Knowler et al., 2014); this definition was adapted such that pre-syringes were excluded from analysis.

Objective measurements of all scans were performed by two unblinded observers (SKS, SDD). For each dog, the 20 bFFE images generated during the cardiac cycle were reviewed, and the two images identified in which the SAD was at its maximum and minimum dimensions, respectively. The dimensions of the SAD were traced on the selected images, allowing for determination of the maximum and minimum area during a cardiac cycle (See Fig. 1). These measurements were performed in the sagittal plane for all dogs (n=12/12) and through transverse segments of the diverticula in seven of 12 dogs. The degree of pulsatile flow within each subarachnoid diverticulum was calculated as the change in area per cardiac cycle (1-minimum area/maximum area).

Criteria for the presence of syringomyelia included a T2W hyperintense, T1W hypointense, and cine bFFE hyperintense lesion within the spinal cord (Ricciardi, 2018). Lesions which appeared isointense on T1W sequences or only mildly hyperintense relative to the spinal cord parenchyma on cine bFFE were classified as pre-syringes or intra-medullary oedema secondary to compressive myelopathy (Ricciardi, 2018) and were not included in this

[1] See: Horos, version 1.1.7., www.horosproject.org (Accessed 29 April 2019)

analysis. The technique described by Rusbridge et al. (2007) was utilised to measure the maximal diameter of each identified syrinx on T2W scans.

Statistical analysis

Data were analysed using a commercial statistical analysis software (SPSS Statistics for OSx, Version 24.0, IBM). All data were found to be non-parametric on Shapiro Wilk test (P<0.05) or skewed on frequency distribution; therefore, only median and range values were calculated for variables of interest, including: age at presentation, maximum and minimum SAD area on sagittal (n=12/12) and transverse (n=7/12) scans, degree of pulsatile flow within each SAD on sagittal (n=12/12) and transverse (n=7/12) scans, and maximum diameter of each syrinx as identified on T2W scan (n=6/12).

A related-samples Wilcoxon signed rank test was utilised to evaluate for significant changes in SAD area on all sagittal and all transverse sequences obtained. The relationship between degree of pulsatile flow and the maximum syrinx diameter was examined on a scatter plot for evidence of correlation; Spearman's rank order correlation coefficient was utilised to screen for significant correlations between SAD pulsation and syrinx size with a $P < 0.05$ considered significant. Intraclass correlation coefficients assessed intra- and inter-observer agreement for all measurements with values <0.40 considered to have poor reliability, values between 0.40-0.59 exhibiting fair reliability and values >0.60 having good reliability ($P < 0.05$; Hallgren, 2012).

Results

Twelve dogs were included in this study. This group consisted of five Pugs, three French bulldogs, one English bulldog, one Rottweiler, one Labrador, and one Staffordshire bull

terrier. Ten males (four neutered) and two females (one neutered) were included; median age was 15.2 months (range, 6 to 118 months). Duration of clinical signs ranged from 24 h to 6 months (median, 2 months) and consisted of progressive proprioceptive ataxia (*n*=11) and ambulatory paraparesis (*n*=6) or tetraparesis (*n*=3), depending on lesion location. Mild mid-cervical spinal hyperaesthesia was reported in one dog. Faecal and/or urinary incontinence was reported at presentation in four dogs. Neuroanatomical localisation included the C1-C5 spinal cord segments in four dogs, C6-T2 in one dog, and the T3-L3 spinal cord segments in the seven remaining cases.

Spinal arachnoid diverticula was diagnosed and localised at C2/C3 in four cases and at C2, T10, T10/T11, T11/T12, T12, T12/T13, T11-T13, and from T8 to L1 in one case each. In all cases, the dilatation was located dorsally to the spinal cord. In two cases, thoracolumbar intervertebral disc protrusions were identified at the site of the SAD.

Pulsation of the SAD was visible on all sagittal and transverse cine bFEE sequences obtained. Analysis of the degree of pulsatile flow on sagittal cine bFFE indicated a median ratio of change in SAD area from minimum to maximum of 0.14 (Table 1). The degree of pulsatile flow observed on transverse cine bFFE was found to exhibit more individual variation, displaying a median ratio of change in SAD cross-sectional area between 0.22-0.24 depending on observer. Both intra- and inter-rater reliability were found to be fair for measurements obtained in the sagittal plane, whereas those in transverse showed good to excellent agreement (Table 1). Significant differences were identified between the median minimum and maximum SAD area dimensions on both sagittal (P=0.002; n=12) and transverse (P=0.018; n=7) sequences on related-samples Wilcoxon signed rank tests for both observers.

Syringomyelia in conjunction with a SAD was observed in 6/12 cases (50%). Syringes were observed just cranial to the SAD in four cases (one cervical and three thoracolumbar), whereas they were noted to extend caudal to the SAD in two cases (one cervical and one thoracolumbar). Excellent intra- and inter-observer agreement was identified on measurements of maximum syrinx diameter (Table 1). No significant association between the degree of pulsation on cine bFFE MRI and the extent of syringomyelia was noted when utilising the averages across all observations or for each observer as an independent assessor (Spearman's rho for averages in sagittal plane = 0.232, P=0.658; in transverse plane rho = - 0.400, P=0.600).

Discussion

Results of the present study provide initial evidence to support the use of cine bFFE sequences as a method for identification and measurement of the dynamic component of canine SAD pulsation on MRI. Pulsation within the SAD throughout the cardiac cycle could be grossly identified in each case on both sagittal and transverse images obtained, and this information was quantitatively measured. The degree of pulsation varied between cases and based upon whether measurements were assessed in the sagittal or transverse plane, yet the difference between minimum and maximum SAD dimensions during the cardiac cycle was found to be significant for measurements made in both planes.

A moderate prevalence of syringomyelia (6/12; 50%) was identified in the current study population in addition to the diagnosis of SAD. Our results indicate that syringes seem to be located more often cranial to a thoracolumbar SAD. Although larger studies are necessary to confirm this finding, a similar relationship has been seen in human medicine. Whether or not this spatial relationship is significant remains unclear; however, it has been hypothesised by Chang et al. (2014) that the presence of a syrinx rostral to an arachnoid adhesion indicates

blockage of caudo-rostral CSF flow, whereas syrinx formation caudal to an arachnoid web will occur secondary to blockage of rostro-caudal CSF flow.

Syringomyelia has been previously hypothesised to occur secondary to blockage of the subarachnoid CSF pathway (Ishizaka et al., 2012; Takeuchi et al., 2003) and abnormal oscillations in CSF flow velocity and pattern (Cerda-Gonzalez et al., 2009; Hentschel et al., 2010). The presence of abnormal CSF flow patterns (e.g. flow jets, turbulent flow) has been previously documented in numerous studies evaluating both Chiari and Chiari-like malformation and spinal arachnoid adhesions using cardiac gated phase contrast MRI (Battal et al., 2011; Cerda-Gonzalez et al., 2009; Chang et al, 2014; Gottschalk et al., 2010; Hentschel et al., 2010; Quon et al., 2015).

A major benefit of phase contrast sequences as compared to cine bFFE lies in the ability to allow for non-invasive quantitative analysis of CSF velocity and identification of flow jets and areas of obstructed flow (Cerda-Gonzalez et al., 2009; Chang et al, 2014; Hentschel et al., 2010; Quon et al., 2015). However, the use of phase contrast sequences alone is limited in the diagnosis of and treatment planning for SAD, as these sequences do not allow for visualisation of arachnoid adhesions (Li et al., 2015). As a result, phase contrast and cine MRI have been utilised together by human neurosurgeons, as the latter sequence provides the high degree of detail and sufficient contrast needed to delineate the arachnoid membrane from the surrounding CSF (Gottschalk et al., 2010; Li et al., 2015). A major limitation of the present study is the absence of concurrent phase contrast sequences, which would allow for confirmation of abnormal flow velocity and/or flow jets within the regions of dynamic SAD pulsation identified on cine MRI.

In the present study, image resolution was not determined to be sufficient to allow for the definitive diagnosis of arachnoid adhesions on cine bFFE sequences, presenting a significant limitation to the potential diagnostic utility of this technique. This may be due to the use of a 1.5 Tesla MRI, as opposed to the 3 Tesla units reported in the human literature. It may also be secondary to the smaller size of the canine vertebral column, which could necessitate a smaller slice thickness or higher in-plane resolution. Additional limitations included the presence of numerous banding artifacts on sagittal cine bFFE sequences, appearing as thick linear hypointensities secondary to magnetic field inhomogeneities (Li et al., 2015). Furthermore, the absence of canine control populations, both healthy and myelopathic, limited the ability to determine whether the identified pulsation was specific to SAD, representing an important area for future research.

Despite these limitations, the improved diagnosis and treatment of canine SAD and arachnoid adhesions remain an important aim in the field of veterinary neurology. Recent work by Tauro et al. (2018) has identified 3D-CISS MRI sequences as significantly improving confidence in the diagnosis of SAD and arachnoid webs, providing enhanced anatomic detail and delineation of SAD from concurrent pathology secondary to altered CSF flow. However, even following accurate diagnosis on advanced imaging and subsequent surgical intervention, it has been shown that neurologic signs may recur for a variety of reasons, including recurrence of the SAD or formation of arachnoid adhesions (Alcoverro et al., 2018). Such findings support the need for additional diagnostics which further our understanding of the pathogenesis of these complex conditions, allowing for advances in the surgical approaches utilised to treat them.

Although none of the advanced imaging modalities discussed may significantly alter diagnosis and treatment when used in isolation, increasing evidence from the field of human

neurosurgery suggests that they may be combined to facilitate early diagnosis and provide targeted therapeutic interventions for improved patient outcome (Chang et al., 2014; Ishibe et al., 2016; Neo et al., 2004; Quon et al., 2015; Yabuki et al., 2007). Several case reports have been described in which cinematic MRI sequences have been used either alone or in conjunction with phase contrast MRI to identify dural defects and regions of abnormal CSF flow which were subsequently closed via laminar fenestration using a minimally invasive approach (Neo et al., 2004; Yabuki et al., 2007). While there remains no agreed upon treatment for cases of concurrent syringomyelia and SAD (Takeuchi et al., 2003), the present work supports the addition of advanced imaging sequences such as cine bFFE to a conventional MRI protocol to heighten understanding of CSF flow dynamics within canine SAD.

Conclusions

This study used cine bFFE MRI to demonstrate the dynamic component of canine SAD pulsation on MRI. Although further studies are necessary to evaluate the clinical relevance of this finding, pulsatile CSF flow is possibly related to the high prevalence of syringomyelia in dogs with SAD.

Conflict of interest statement

None of the authors of this paper have a financial or personal relationship with other people or organisations that could inappropriately influence or bias the content of the paper.

Appendix A: Supplementary material

Supplementary cine bFFE MRI video images associated with this article may be found in the online version, at doi: …

References

Alcoverro, E., McConnell, J. F., Sanchez-Masian, D., De Risio, L., De Decker, S., Gonçalves, R., 2018. Late-onset recurrence of neurological deficits after surgery for spinal arachnoid diverticula. Veterinary Record 182, 380.

Battal, B., Kocaoglu, M., Bulakbasi, N., Husmen, G., Tuba Sanal, H., Tayfun, C., 2011. Cerebrospinal fluid flow imaging by using phase-contrast MR technique. The British Journal of Radiology 84, 758-765.

Bentley, J.F., Simpson, S.T., Hathcock, J.T., 1991. Spinal arachnoid cyst in a dog. Journal of the American Animal Hospital Association 27, 549-551.

Cerda-Gonzalez, S., Olby, N.J., Broadstone, R., McCullough, S., Osborne, J.A., 2009. Characteristics of cerebrospinal fluid flow in Cavalier King Charles Spaniels analysed using phase velocity cine magnetic resonance imaging. Veterinary Radiology & Ultrasound 50, 467-476.

Chang, H.S., Nagai, A., Oya, S., Matsui, T., 2014. Dorsal spinal arachnoid web diagnosed with the quantitative measurement of cerebrospinal fluid flow on magnetic resonance imaging. Journal of Neurosurgery: Spine 20, 227-233.

Driver, C.J., Volk, H.A., Rusbridge, C., Van Ham, L.M., 2013. An update on the pathogenesis of syringomyelia secondary to Chiari-like malformation in dogs. The Veterinary Journal 198, 551-559.

Driver, C.J., Watts, V., Bunck, A.C., Van Ham, L.M., Volk, H.A., 2013. Assessment of cerebellar pulsation in dogs with and without Chiari-like malformation and syringomyelia using cardiac-gated cine magnetic resonance imaging. The Veterinary Journal 198, 88-91.

Dyce, J., Heritage, M. E., Houlton, J. E., Palmer, A. C., 1991. Canine spinal 'arachnoid cysts'. Journal of Small Animal Practice 32, 433-437.

Gage E. D., Hoerlein B.F., Bartels J.E., 1968. Spinal cord compression resulting from a leptomeningeal cyst in the dog. Journal of the American Veterinary Medical Association 152, 1664–1670.

Galloway, A. M., Curtis, N. C., Sommerlad, S. F., Watt, P. R., 1999. Correlative imaging findings in seven dogs and one cat with spinal arachnoid cysts. Veterinary Radiology & Ultrasound 40, 445-452.

Gnirs, K., Ruel, Y., Blot, S., Begon, D., Rault, D., Delisle, F., Boulouha, L., Colle, M., Carozzo, C., Moissonnier, P., 2003. Spinal sub arachnoid cysts in 13 dogs. Veterinary Radiology & Ultrasound 44, 402-408.

Gottschalk, A., Schmitz, B., Mauer, U.M., Bornstedt, A., Steinhoff, S., Danz, B., Schöltzer, W., Rasche, V., 2010. Dynamic visualization of arachnoid adhesions in a patient with idiopathic syringomyelia using high-resolution cine magnetic resonance imaging at 3T. Journal of Magnetic Resonance Imaging 32, 218-222.

Hallgren, K., 2012. Computing inter-rater reliability for observational data: An overview and tutorial. Tutor Quant Methods Psychol 8, 23-34.

Hentschel, S., Mardal, K.-A., Løvgren, A.E., Linge, S., Haughton, V., Characterization of cyclic CSF flow in the foramen magnum and upper cervical spinal canal with MR flow imaging and computational fluid dynamics. American Journal of Neuroradiology 31, 997-1002.

Holly, L., T., Batzdorf, M., 2006. Syringomyelia associated with intradural arachnoid cysts. Journal of Neurosurgery: Spine 5, 111-116.

Ishibe, T., Senzoku, F., Kamba, Y., Ikeda, N., Mikawa, Y., 2016. Time-spatial labelling inversion pulse magnetic resonance imaging of cystic lesions of the spinal cord. World Neurosurgery 88, 693.E13-693.E21.

Ishizaka, S., Hayashi, K., Otsuka, M., Fukuda, S., Tsunoda, K., Ushijima, R., Kitagawa, N., Suyama, K., Nagata, I., 2012. Syringomyelia and arachnoid cysts associated with spinal arachnoiditis following subarachnoid hemorrhage. Neurologia Medico-Chirurgica 52, 686-690.

Kim, M., Kim, S., 2009. Syringomyelia associated with a spinal arachnoid cyst. Journal of Korean Neurosurgical Society 45, 315-317.

Knowler, S.P., McFadyen, A.K, Freeman, C., Kent, M., Platt, S.R., Kibar, Z., Rusbridge, C., 2014. Quantitative analysis of Chiari-like malformation and syringomyelia in the Griffon Bruxellois Dog. PLoS ONE 9, e88120.

Li, A.E., Wilkinson, M.D., McGrillen, K.M., Stoodley, M.A., Magnussen, J.S., 2015. Clinical applications of cine balanced steady-state free precession MRI for the evaluation of the subarachnoid spaces. Clinical Neuroradiology 25, 349-360.

Lowrie, M.L., Platt, S.R., Garosi, L.S., 2014. Extramedullary spinal cysts in dogs. Veterinary Surgery 43, 650-662.

Mauler, D.A., De Decker, S., De Risio, L., Volk, H.A., Dennis, R., Gielen, I., Van der Vekens, E., Goethals, K., Van Ham, L., 2014. Signalment, clinical presentation, and diagnostic findings in 122 dogs with spinal arachnoid diverticula. Journal of Veterinary Internal Medicine 28, 175-181.

Neo, M., Koyama, T., Sakamoto, T., Fujibayashi, S., Nakamura, T., 2004. Detection of a dural defect by cinematic magnetic resonance imaging and its selective closure as a treatment for a spinal extradural arachnoid cyst. Spine (Phila PA) 29, E426-E430.

Parker, A.J., Adams, W.M., Zachary, J.F., 1983. Spinal meningeal cysts in the dog. Journal of the American Animal Hospital Association 19,1001–1008.

Quon, J.L., Grant, R.A., DiLuna, M.L., 2015. Multimodal evaluation of CSF dynamics following extradural decompression for Chiari malformation Type I. Journal of Neurosurgery: Spine 22, 622-630.

Ricciardi, M., 2018. Principles and applications of the balanced steady-state free precession sequence in small animal low-field mri. Vet Res Commun 42, 65-86.

Rylander, H., Lipsitz, D., Berry, W.L., Sturges, B.K., Vernau, K.M., Dickinson P.J., Anor, S.A., Higgins, R.J., LeCouteur, R.A., 2002. Retrospective analysis of spinal arachnoid cysts in 14 dogs. Journal of Veterinary Internal Medicine 16, 690–696.

Rusbridge, C., Carruthers, H., Dube, M.P., Holmes, M., Jeffery N.D., 2007. Syringomyelia in Cavalier King Charles spaniels: the relationship between syrinx dimensions and pain. Journal of Small Animal Practice 48, 432-436.

Skeen, T.M., Olby, N.J., Muñana, K.R., Sharp, N.J., 2003. Spinal arachnoid cysts in 17 dogs. Journal of the American Animal Hospital Association 39, 271-282.

Takeuchi, A., Miyamoto, K., Sugiyama, S., Saitou, M., Hosoe, H., Shimizu, K., 2003. Spinal arachnoid cysts associated with syringomyelia: Report of two cases and a review of the literature. Journal of Spinal Disorders & Techniques 16, 207-211.

Tauro, A., Jovanovik, J., Driver, C.J., Rusbridge, C., 2018. Clinical applications of 3D-CISS MRI sequences for diagnosis and surgical planning of spinal arachnoid diverticula and adhesions in dogs. Veterinary and Comparative Orthopaedics and Traumatology 31, 83-94.

Yabuki, S., Kikuchi, A., 2007. Multiple extradural arachnoid cysts: Report of two operated cousin cases. Spine 32, E585-E588.

Figure legends

Fig. 1. Sagittal (C and D) and transverse (A and B) cine bFFE MRI of a 9-year-old male neutered Pug with SAD at the level of T12/T13. Maximum (B and D) and minimum (A and C) area dimensions of the SAD outlined in green. An increase in SAD area is seen throughout the cardiac cycle on both sagittal and transverse sequences.

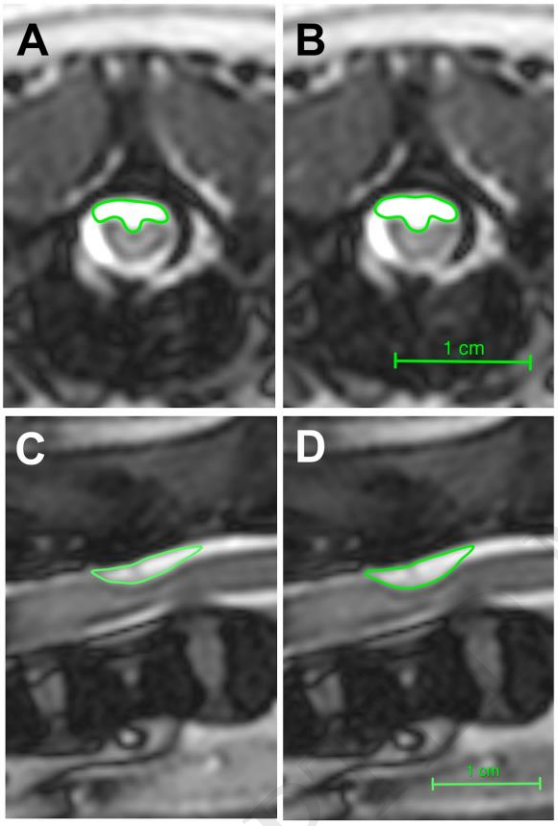

Table 1

Primary outcome measures reported as medians with range in parentheses below for each observer. Intra- and inter-rater reliability for each parameter listed as intraclass correlation coefficients (ICC) to the right (statistical significance of each ICC below).

	Observer 1 (SKS)	Observer 2 (SDD)	Intra-rater reliability	Inter-rater reliability
Ratio of change in SAD area (sagittal)	0.14 (0.10-0.27)	0.14 (0.07-0.36)	0.483 (*P*=0.47)	0.596 (*P*=0.016)
Ratio of change in SAD area (transverse)	0.22 (0.05-0.53)	0.24 (0.07-0.41)	0.906 (*P*=0.001)	0.705 (*P*=0.025)
Syrinx diameter on T2 weighted transverse	3.7 mm (2.5-5.6)	3.8 mm (2.9-5.9)	0.975 (*P*=0.001)	0.935 (*P*=0.001)

SKS, S.K. Shivapour; SDD, S. De Decker; SAD, spinal arachnoid diverticulae.